Structure of the Light-Driven Chloride Pump Halorhodopsin at 1.8 Å Resolution

Michael Kolbe, Hüseyin Besir, Lars-Oliver Essen,* Dieter Oesterhelt*

Halorhodopsin, an archaeal rhodopsin ubiquitous in Haloarchaea, uses light energy to pump chloride through biological membranes. Halorhodopsin crystals were grown in a cubic lipidic phase, which allowed the x-ray structure determination of this anion pump at 1.8 angstrom resolution. Halorhodopsin assembles to trimers around a central patch consisting of palmitic acid. Next to the protonated Schiff base between Lys^{242} and the isomerizable retinal chromophore, a single chloride ion occupies the transport site. Energetic calculations on chloride binding reveal a combination of ion-ion and ion-dipole interactions for stabilizing the anion 18 angstroms below the membrane surface. Ion dragging across the protonated Schiff base explains why chloride and proton translocation modes are mechanistically equivalent in archaeal rhodopsins.

Anion transport through biological membranes is less well understood than proton transport, classic examples of the latter being the proton pumps F0F1–adenosine triphosphatase and bacteriorhodopsin (*1*, *2*). Whereas several anion exchangers have been discovered and functionally characterized in eukaryotic and bacterial membranes, only a few anion pumps have been reported, e.g., an adenosine triphosphate–driven arsenate transporter (*3*) and a chloride pump from the marine alga *Acetabularia* (*4*). To date, halorhodopsin (HR) is the only known anion pump that is energized by light (*2*, *5*). HR occurs ubiquitously in halophilic archaea and mediates primarily chloride (*6*), but also bromide, iodide, and nitrate import into the cell against their electrochemical gradients. Extremely halophilic archaea thrive in saturated brines with isoosmolar salt concentrations in their cytoplasm. Here, light energy contributes substantially by HR to maintain an osmotic balance during cell growth.

Halorhodopsin belongs to a subfamily of heptahelical membrane proteins, the archaeal rhodopsins, as shown by sequence homology to bacteriorhodopsin (BR) and sensory rhodopsins or, structurally, by electron crystallography on two-dimensional (2D) crystals (*7*). HR binds retinal covalently as a protonated Schiff base (PSB) to its only lysine residue, Lys^{242} in helix G. The Schiff base and a shell of surrounding amino acids form the active center that absorbs green light with a maximum wavelength (λ_{max}) of 578 nm. Here, photon absorption triggers a catalytic cycle by an all-trans to 13-cis isomerization of the retinal chromophore in less than 10 ps (*8*). An ongoing sequence of slower thermal reactions comprising reisomerization, ion transfer steps, and changes in the accessibility of a transport center toward the extracellular and cytosolic side leads to the net transport of one chloride per photon toward the cytosol.

As an anion pump, HR provides a paradigm for other, functionally diverse chloride transporters such as the erythrocyte Cl^-/HCO_3^- exchanger, the Na^+/K^+-chloride cotransporters, and the cystic fibrosis transmembrane conductance regulator chloride channel. At first glance, chloride transport through these membrane proteins should set different structural restraints on suitable translocation pathways than proton transport. The latter preferably occurs along internal H-bonding chains consisting of water molecules and protonable side chains where structural changes are not required for transport per se but only for unidirectionality and energy conservation. In contrast, chloride ions (Pauling radius = 1.81 Å) are sterically demanding and impose high energetic penalties on desolvation. Nevertheless, the architecture of archaeal rhodopsins is compatible with the transport of both species, chloride and protons, as shown by HR (*9*) and the single site mutants $Asp^{85} \rightarrow$ Thr(Ser) of BR (*10*, *11*). To resolve this perplexing issue, we determined the high-resolution structure of HR complexed to chloride.

Crystallization and HR structure. We crystallized HR in a cubic monoolein-water-KCl phase under conditions that mimic the hypersaline conditions of the haloarchaeal cytosol in the aqueous subphase (*12*). Structure determination by molecular replacement (Table 1) succeeded with a model of halorhodopsin that was based on a previous structure of BR (*13*). Recently, crystallization in cubic lipidic phases (CLP) (*14*) was suggested to proceed through a transition of the lipidic component from a cubic to a lamellar L_α-like phase (*15*). The 3D structure of HR from CLP-grown crystals corroborates this notion by showing a similar layered arrangement of HR trimers (Fig. 1, A and B) like in CLP-grown BR crystals (*16*, *17*). Ten lipids interspersed between the HR trimers assemble to small hexagonal patches with average interlipid spacings of 4.5 to 4.7 Å. These spacings are characteristic for lamellar L_α phases of monoalkyl compounds like monoolein (*18*) but not for the branched, phytanol-containing lipids of haloarchaea. Apparently, the tendency of monoolein to form L_α-like phases at low hydration levels suffices to drive the hexagonal arrangement of embedded HR trimers.

HR adopts the architecture of an archaeal rhodopsin as exemplified before by BR. Despite the differences in ion specificity and transport vectoriality, the transmembrane region of HR is structurally well conserved as shown by a superposition on BR from *Halobacterium salinarum* that shares 31% sequence identity with HR. Structural similarity is highest for the pentahelical bundle C-G, resulting in a root mean square deviation (rmsd) of only 0.74 Å for 122 C_α positions. When superimposing HR and BR along this bundle, helices A and B become blockwise dislocated by 2.1 and 1.3 Å, respectively (Fig. 2B). Together with a larger sequence diversity for helices A and B in other archaeal rhodopsins (*19*) and the residence of the chromophore between helices C to G, it is conceivable that the 5-TM bundle C-G represents a conserved, minimal core of archaeal rhodopsins.

The extracellular surface of HR is dominated by its BC loop, which is 6 to 16 residues longer in halorhodopsins than in BR (*5*). The BC loop starts off as two antiparallel paired β strands (Gln^{87}-Met^{91}, Glu^{100}-Ser^{104}) and extends along the whole extracellular side of HR contacting the ends of helices C-G (Fig. 3A). The connecting segment (Pro^{92}-Ala^{98}) forms a complex loop and is anchored at its tip by a highly conserved histidine, His^{95}. Buried from solvent access, His^{95} makes branched H bonds to the carbonyls of Val^{218} and Gly^{220} on the FG loop. A structural role for His^{95} is supported by the $His^{95} \rightarrow$ Arg mutant, which showed impaired stability under light-exposed conditions (*20*). The charge distribution on the extracellular side of HR suggests that anions could bind to the surface close to residue Arg^{103} (Fig. 3B). However, Arg^{103} at the root of the BC loop is not conserved among halorhodopsins (*5*) from other species. On the cytoplasmic side, the COOH-terminus of HR (Asn^{256}-Ala^{262}) folds into the short helix G′ running almost parallel to the membrane plane between the loops AB and EF. Arg^{258} on helix G′ forms with four other arginines on the AB loop (Arg^{52}, Arg^{55}, Arg^{58}, and Arg^{60}), a highly positively charged surface patch (Fig. 3C). Chloride binding was observed neither in this region nor on the extracellular surface despite chloride concentrations exceeding 3

Department of Membrane Biochemistry, Max-Planck-Institute for Biochemistry, Am Klopferspitz 18a, D-82152 Martinsried bei München, Germany.

*To whom correspondence should be addressed. E-mail: essen@biochem.mpg.de or oesterhe@biochem.mpg.de.

M in the crystals. A putative role for the arginine cluster might be to generate a strong electrical field between the transport site and the cytoplasmic surface and to enforce chloride transfer during the catalytic cycle. Recent measurements on the chloride concentration dependency of the electrogenic HR activity indicated that chloride binding on the surfaces of HR is indeed very weak, with estimated binding constants of 6 M for the extracellular and 7.5 M for the cytosolic side (*21*).

Active center and transport site. The retinal chromophore is found in an all-trans, 15-anti configuration (Fig. 4A), as previously demonstrated by resonance-Raman spectroscopy on HR (*22*). The presence of a single, well-ordered chloride ion, CL501, next to the Schiff base nitrogen indicates that the primary ion transport site of HR is closely associated with the isomerizable chromophore. As viewed in Fig. 5A, the solvation sphere of CL501 is irregular and contains 15 hydrogen and 3 nonhydrogen atoms. The preponderance of hydrogen atoms in the solvation sphere derives mainly from the aliphatic groups that contact the halide and an associated water cluster comprising WAT505, WAT508, and WAT512 (Fig. 4, B and C). Chloride CL501 accepts hydrogen bonds only from WAT508 (3.14 Å), WAT512 (3.21 Å), and Ser^{115} (3.07 Å), whereas 10 hydrogen atoms belong to the methylene groups of Ser^{73}, Ser^{76}, and Ser^{115}, the CD1 atom of the indole moiety of Trp^{112}, and the terminal methyl groups of Val^{72} and Thr^{111}. The precise arrangement of the latter residues might influence the affinity of the chloride binding site as suggested by the modest effects of the $Thr^{111} \rightarrow$ Val mutation on transport activity (*23*).

Despite contacting the chloride (Lys^{242} NZ-CL501 3.75 Å), the PSB is unfavorably oriented to make regular hydrogen bonds with CL501 or any other group; e.g., an H bond between CL501, the Schiff base proton, and nitrogen would be strongly bent with an angle of 105°. The close association between the PSB and chloride (Fig. 5A) explains the observed anion-dependent shifts of PSB-specific Fourier transform infrared spectroscopy (FTIR) bands (*24*). Furthermore, a strong electrostatic control of the pK_a (where K_a is the acid constant) of the Schiff base by bound chloride is indicated by electro-

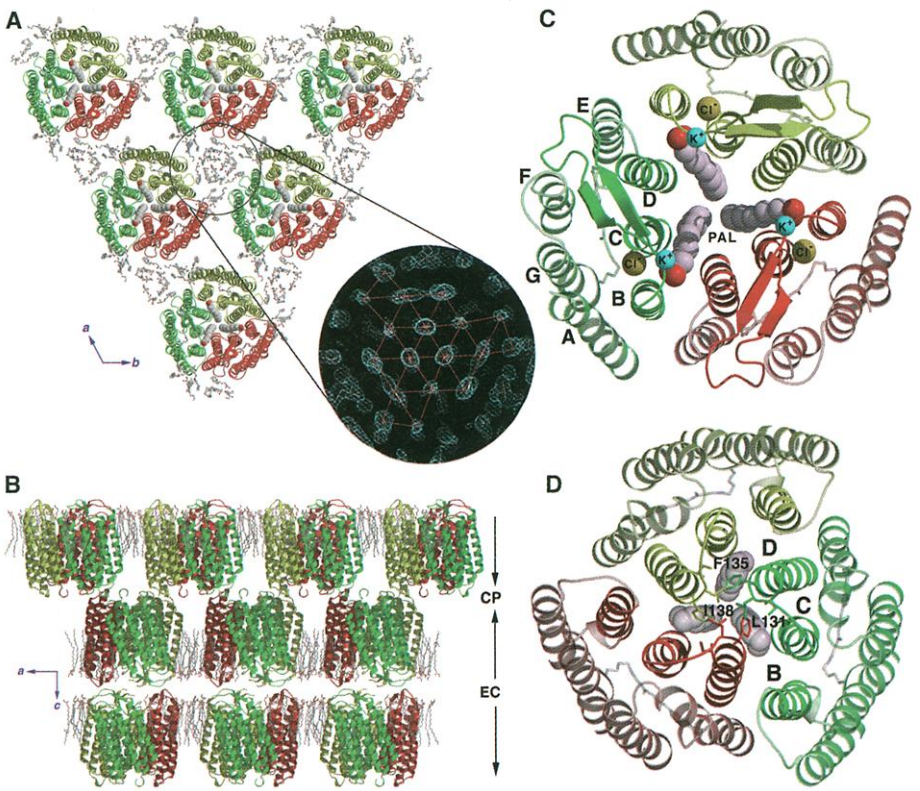

Fig. 1. Quaternary structure and crystal packing of HR. (**A**) Arrangement of HR/lipid trimers in layers parallel to the *ab* plane. The inset shows SIGMAA-weighted $2F_{obs} - F_{calc}$ electron density for the intertrimer lipid patches (contouring level: 0.8σ). Lipids between HR trimers were modeled as monoolein. Only two of them showed corresponding electron density for the glycerol moiety; the others are only partially defined by electron density as reflected by appropriately set occupancies. For clarity, HR monomers are shown as red, yellow, and green ribbon models. (**B**) Perpendicular view showing the layer packing along the *c* direction. Crystal contacts in the *ab* plane are exclusively derived from protein-lipid-protein interactions, whereas direct protein-protein interactions occur only in the *c* direction, mainly by symmetric contacts involving the AB and BC loops and the COOH-termini of symmetry-related molecules. (**C**) View on the trimeric halorhodopsin-lipid complex from the extracellular side (EC). Palmitates (PAL), potassium (cyan), and chloride ions (yellow) are shown as space-filling CPK models. (**D**) View on the HR/lipid trimer from the cytoplasmic side (CP). The C10-C16 hydrocarbon tails of the palmitates end in a narrow channel that is walled by Ala^{113}, Pro^{117}, Ala^{139}, and Ile^{142} (*34*). Together with the highlighted residues Leu^{131}, Phe^{135}, and Ile^{138}, a hydrophobic plug is formed in the CP half of the HR trimer whose dense packing seals the extracellular from the intracellular space. For comparison, the internal compartment of the BR trimer is cylindrically shaped and sealed by a lipidic patch on the EC half consisting of the archaeal glycolipid S-TGA-1. This figure and Figs. 2 to 4 were prepared with MOLSCRIPT and RASTER-3D (*35*).

Table 1. Crystal structure determination and refinement. X-ray data were collected from single flash-frozen HR crystals at 100 K. Intensity data were reduced with MOSFLM6.0 (*41*) and SCALA (*42*). HR crystals diffract to 1.8 Å resolution, belong to space group $P6_322$ ($a = b = 67.3$ Å, $c = 209.2$ Å), and comprise one monomer per asymmetric unit. The structure of HR was solved by molecular replacement with CNS (*43*). The search model, the BR structure 1BRR (*13*) (residues 9 to 67, 78 to 152, and 167 to 223), was corrected to the HR sequence at 34 positions and set to alanine at 69 positions with INSIGHT II (Molecular Simulations). The solution found with this hybrid model gave a correlation coefficient (CC) of 0.468 in the translation search (used data: 15 to 4.8 Å, CC of next peak: 0.383). Rigid-body refinement followed by simulated annealing and torsion angle dynamics in CNS (starting temperature = 6000 K, change in temperature = 35 K, data: 25 to 2.4 Å) gave an *R* factor/R_{free} of 40.3/43.7%. The initially omitted BC and EF loops were stepwise rebuilt during subsequent refinement rounds. No contribution from a dark-adapted 13-cis, 15-syn retinylidene was observed for the chromophore in difference electron density maps, although light-adapted HR is reported to contain about 20% of this chromophore species (*44*). Omit maps were regularly calculated to check functionally important regions, e.g., the transport site or helix distortions. The final model consists of 2099 atoms and exhibits good stereochemistry as analyzed by PROCHECK (*45*).

Data collection	
Beamline, wavelength	ID14-3 (ESRF), 0.93 Å
Resolution	25–1.8 Å
Unique reflections	26590
Multiplicity	6.6 (5.1)*
Mosaicity, Wilson *B* factor	0.42°, 26.2 Å²
$I/\sigma(I)$	26.5 (2.8)*
R_{merge}†	0.051 (0.313)*
Completeness	98.2 % (92.3 %)*
Refinement statistics	
Resolution	25–1.8 Å
No. of reflections working/free	24896, 1617
R factor/R_{free}†	0.237, 0.257
rmsd for bonds, angles	0.018 Å, 1.77°
Protein residues, lipids, ions, and waters	239, 11, 2, 96

*Statistical values in parentheses correspond to the highest resolution shell (1.9 to 1.8 Å). †$R_{merge} = \Sigma_{hkl}\Sigma_i|I_i(hkl) - \langle I(hkl)\rangle|/\Sigma_{hkl}\Sigma_i I_i(hkl)$, where *I* is the measured intensity. ‡*R* factor = $\Sigma||F_{obs} - F_{calc}||/\Sigma F_{obs}$, where F_{obs} and F_{calc} are the observed and calculated structure factors, respectively; R_{free} calculated with 6% of the data.

static calculations (Table 2) and ultraviolet/visible spectroscopy that shows a drop of the Schiff base pK_a by at least 1.5 units when lowering the chloride concentration (*25*). Compared with the transport site in BR, the chloride occupies an almost identical position as the OD1 atom of Asp^{85} in BR ($\Delta x = 0.34$ Å). This coincidence is contrasted by differing positions for the associated water clusters and the helix backbone around Thr^{111}, which is distorted in HR by adopting a 3_{10}-like turn (Leu^{110}-Ala^{113}). WAT508 bridges between CL501 and the carboxylate of Asp^{238} (Fig. 4C). According to electrostatic calculations, Asp^{238} is like its counterpart in BR, Asp^{212}, deprotonated, although its $pK(1/2)$ is strongly affected by chloride binding (Table 2). The guanidinium group of Arg^{108} was previously inferred to represent the chloride binding site; neutral mutants of Arg^{108} were completely defective in chloride transport but could be restored by adding guanidinium salts (*26*). The observed distance of 7.4 Å between CL501 and the guanidinium group of Arg^{108} shows that the stabilizing effect of Arg^{108} is mostly indirectly effected through the intervening water cluster. Consequently, the complex counterion of the PSB, comprising in BR the residues Asp^{85}, Asp^{212}, and Arg^{82} (*2*), is replaced in HR by CL501, Asp^{238}, and Arg^{108}.

Although discontinuous from the extracellular side, a pathway between the transport site and the extracellular surface can easily be formed if Arg^{108} undergoes a conformational change during the photocycle. Its guanidinium group makes an H bond with the side chain of Gln^{105} residing above. The latter residue is not conserved in other halorhodopsins but might affect the conformational flexibility of Arg^{108} and thereby anion uptake, as indicated by the $Gln^{105} \rightarrow$ Glu exchange that causes a delayed uptake (*23*). This entrance for chloride above Gln^{105}-Arg^{108} appears to have a similar hydrophobic surface character as the internal chloride binding site. Its walling, a greasy edge comprising five hydrophobic residues, Leu^{29}, Leu^{33}, Leu^{80}, Val^{86}, and Val^{227}, is highly conserved in halorhodopsins and might support partial desolvation of chloride already on the protein surface (Fig. 3A). In contrast, no chloride-conducting pathway extending from the PSB toward the cytosolic surface of HR is found because of protein packing. Conformational changes required to open such a pathway possibly involve the COOH-terminal end of helix E. This helix is distorted by a π bulge between residues Ala^{178} and Trp^{183} and can also be found in BR (*13*). The helix segment Thr^{181}-Gly^{191} not only ex-

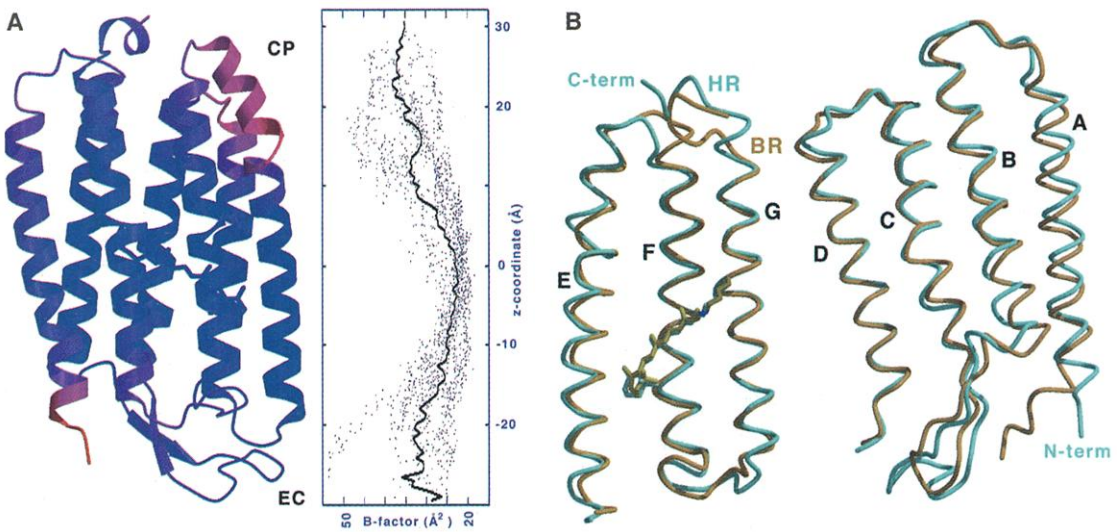

Fig. 2. **(A)** Distribution of thermal B factors in HR ranging from 18.4 Å² (blue) to 80.9 Å² (red). The diagram shows the B factor distribution along the z axis, which corresponds to the normal of the HR/lipid layer. As judged from the minimum of the B factor distribution along the membrane normal, the retinal and its surroundings form a rigid core in HR. This rigidity is also intrinsic for BR as shown by neutron diffraction and might be important for the efficient photoreceptor function of all archaeal rhodopsins (*36*). **(B)** Structural comparison between the C_α traces of HR (cyan) and BR (yellow, Protein Data Bank code 1QHJ). Compared with BR, the retinal is only slightly displaced, starting from 0.4 Å at the PSB to 0.8 Å at the ionone ring.

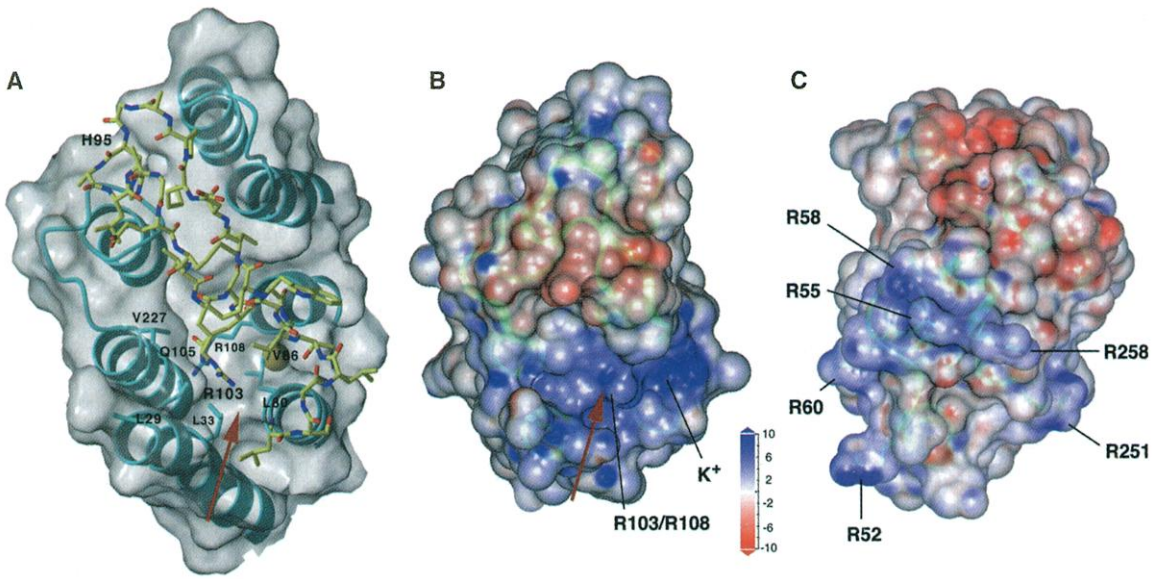

Fig. 3. Extramembranous surfaces of HR. **(A)** Packing of the BC loop on the extracellular side of HR. The putative entrance site for chloride, the greasy edge, is indicated by a red arrow. **(B)** Electrostatic surface potentials on the extracellular side of HR. **(C)** The same on the cytoplasmic side. Electrostatic potentials ranging from −10 kcal/mol (red) to +10 kcal/mol (blue) were calculated with DELPHI with partial charges as described in Table 2 and mapped onto a surface-accessible surface as computed by INSIGHTII with a 1.4 Å probe.

hibits increased thermal mobility (Fig. 2A) but resides just above Thr[203] (Fig. 4A), the putative chloride acceptor on the cytoplasmic side of the chromophore (*23*).

Electrostatics in the halide transport site. The transport site of HR is located 18 Å below the extracellular membrane surface; i.e., the chloride gets stuck approximately halfway on its course through the membrane. As lipid bilayers are low-dielectricity barriers for ion translocation, we wondered which features of the transport site contribute mostly to chloride binding. Free energies for transferring chloride from bulk water ($\varepsilon = 80$) to the transport site were calculated with the full-atomic model of HR with internally bound waters and the assumption that HR is embedded in an apolar membrane context (Fig. 5B). When turning on all partial charges, chloride transfer is energetically slightly favorable with the change in Gibbs free energy $\Delta G = -1.3$ kcal/mol; the corresponding dissociation constant of 0.1 M is in the range of reported transport affinities. In contrast, the same transfer without any charges on the protein and buried waters costs +20.3 kcal/mol (Fig. 5C). The discrepancy of −21.6 kcal/mol arises from stabilizing interactions between CL501 and the electrostatic field generated by the protein microenvironment. Besides the set of surface-exposed acidic and basic residues, the ion pair PSB-Asp[238] adds the least to chloride binding ($\Delta\Delta G = -2.4$ kcal/mol). The pairing of CL501 with the PSB group, which, by itself, accounts for −13 kcal/mol, is almost balanced by electrostatic repulsion with the negatively charged carboxylate of Asp[238]. Consequently, minor distortions in the electrostatic coupling between chloride and the PSB occurring after photoisomerization might destabilize bound chloride. A stronger ion-ion interaction is made with the more distant guanidinium group of Arg[108]. Here, the ion pair Arg[108]-Glu[219] stabilizes

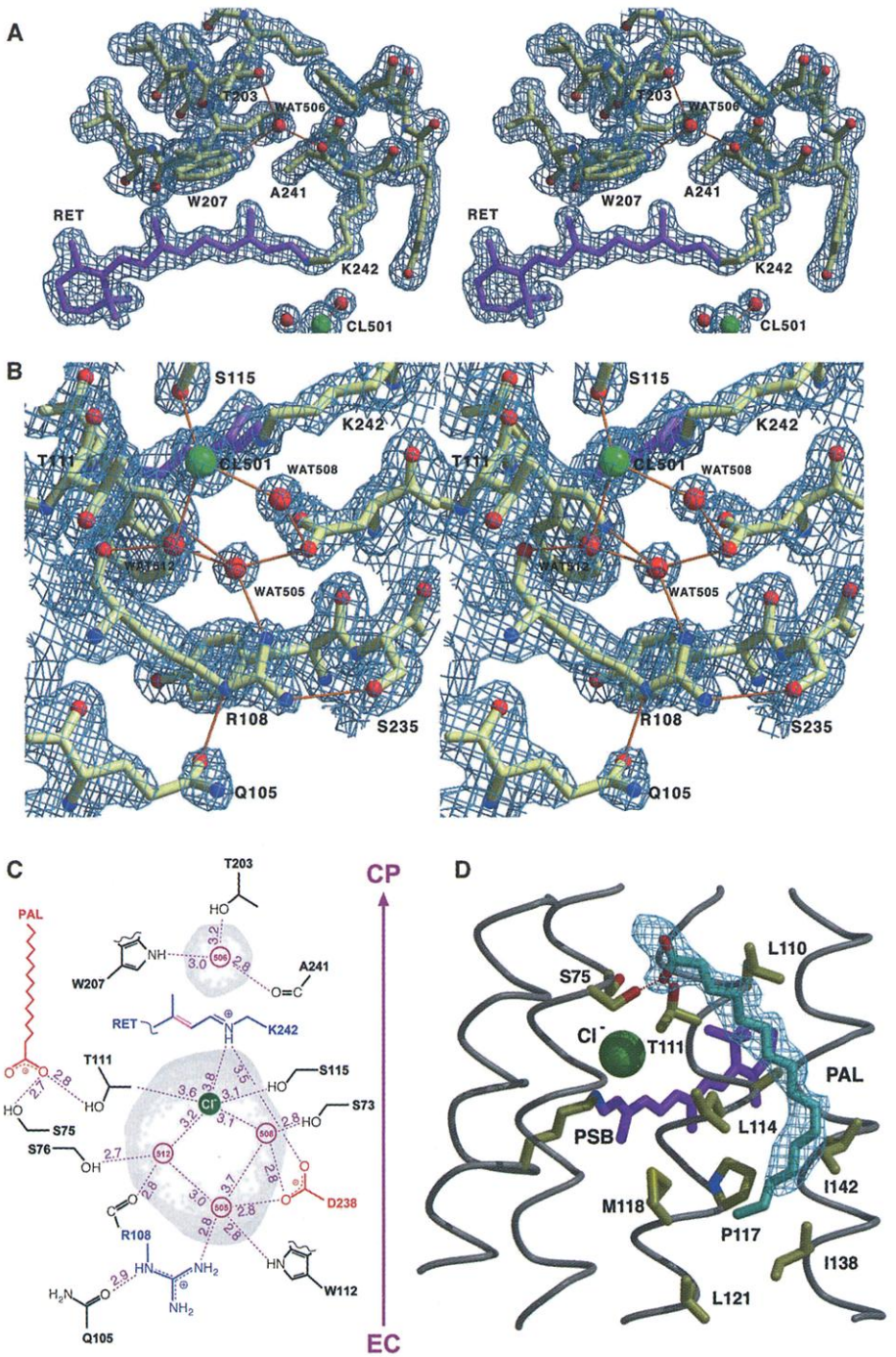

Fig. 4. The retinal and chloride binding site. (**A**) The cytoplasmic side of the retinal chromophore. The Schiff base is separating the extracellular access channel (bottom) from the cytoplasmic half of HR. The retinal binding site in HR is walled by 16 residues; nine of them are strictly conserved among all archaeal rhodopsins (*19*), whereas differences between the ion pumps HR and BR are only found at five positions (Ser[115], Ile[119], Trp[165], Cys[169], and Phe[172]). The structurally conserved water WAT506 is highlighted. (**B**) The chloride-water cluster at the extracellular side. Putative hydrogen bonds are shown in orange. The SIGMAA-weighted $2F_{obs} - F_{calc}$ electron density maps in (A) and (B) (cyan) are contoured at 1σ. Prior to inclusion into the model, the peak height of the $F_{obs} - F_{calc}$ omit density was 108 σ for CL501 and 4.2 σ for the accompanying WAT508. Around Lys[242], the G helix is distorted by adopting a π bulge conformation (Phe[240]-Ala[245]) like previously described for BR (*16*). (**C**) Scheme depicting the hydrogen-bonding pattern between the transport site and the extracellular surface of HR. The volumes of internal cavities that hold CL501 and its associated water cluster or WAT506 (gray shading) are 67 Å^3 and 21 Å^3, respectively. The isomerizable 13-14 bond of the retinal is highlighted in purple; distances are given in angstroms. (**D**) Binding of palmitate close to the transport site. The $2F_{obs} - F_{calc}$ SA-OMIT electron density for palmitate is contoured at 0.8σ. The side-chain conformation of Thr[111] that H bonds to the palmitate and thus faces CL501 by its methyl group is unambiguously defined by electron density. Palmitate is not synthesized by Haloarchaea but is ubiquitous in their natural habitat and growth media. Tritium-labeled palmitate added during the cultivation of *H. salinarum* strain D2 comigrates with HR during purification (*37*). Likewise, matrix-assisted laser desorption/ionization–mass spectrometry analysis indicates the presence of palmitate in HR samples used for crystallization (*38*).

bound chloride by −4.6 kcal/mol without major adversary effects from Glu^{219}. The energetic coupling between Arg^{108} and CL501 correlates with FTIR data showing a dependence of the C–N vibrations in the guanidinium group on the bound halide species (*27*). Although ion-ion interactions sum up to −8.3 kcal/mol, a similar amount, −8.9 kcal/mol, accounts for the dipole-ion interactions between CL501, the water molecules WAT508 and WAT512, and the hydroxyl group of Ser^{115}. Partial solvation of chloride by two water molecules might restrain the extent to which chloride accommodates changes in its environment during a light-driven pump cycle. Finally, the aliphatic hydrogen atoms whose dipole moments along the C–H bonds are about five times weaker than the O–H dipoles of polar hydrogen atoms are collectively important ($\Delta\Delta G$ = −4.5 kcal/mol). It is mostly this set of interactions that is not structurally reproduced in the chloride-pumping BR mutant $Asp^{85} \rightarrow$ Thr because of sequence differences and the slightly different placement of helix B at the transport site. Despite mimicking the spectroscopy of HR (*11*), the $Asp^{85} \rightarrow$ Thr mutant exhibits a much weaker binding constant for chloride, about 2 M, than HR (Michaelis constant $K_M \approx$ 8 to 40 mM).

Table 2. Electrostatic calculations. p*K*(1/2) values for titratable residues were estimated from electrostatic calculations with the quasi-macroscopic model in MEAD, version 1.1.8 (*39*). Hydrogen atoms and partial charges were added from the DISCOVER force field (Molecular Simulations); the hydroxyls of Ser, Thr, Tyr, and waters were oriented by PROTEUS [distributed as part of the GRASP package (*46, 47*)] with recommended parameters. Partial charges for the Schiff base-retinal moiety used the parameter set from Tavan *et al.* (*48*). Multiple site titration used Monte Carlo sampling as performed by the program xmcti (*49*). pK_a values for the Schiff base that were determined in the dark are shown in parentheses (*25*).

Residue	p*K*(1/2), with Cl^-	p*K*(1/2), w./o. Cl^-
Arg^{103}	11.0	11.0
Arg^{108}	15.0	13.0
Asp^{141}	11.7	12.7
Glu^{219}	2.5	2.6
Asp^{238}	4.8	−2.0
Schiff base	19.8 (8.9)	7.3 (7.4)
Palmitate	4.5	4.5

The HR-trimer/lipid complex. Both archaeal rhodopsins, HR and BR, form trimers that separate an internal compartment from the surrounding bulk lipid phase. However, remarkable differences are found for the protomer orientations in the membrane; HR is tilted by 11° when compared with BR. Consequently, the internal compartment encircled by the HR trimer opens toward the extracellular side like a funnel. The intratrimer contacts are mainly made between the BC and CD helix pairs of neighboring molecules and occlude 1057 Å^2 surface area per monomer. In contrast, BR chooses a different mode for trimerization. Here, only the B and D helices associate with each other and occlude a much smaller surface area from solvent access (659 Å^2). Inside the HR trimer, a lipidic species, the fatty acid palmitate, was delineated by electron density (Fig. 4D). Three palmitates reside in the middle of the HR trimer (Fig. 1C), their carboxylates about 10 Å below the surface plane of the bulk lipid phase as represented by the microcrystalline monoolein patches. The carboxylates are H bonded to the hydroxyls of Ser^{75} and Thr^{111} (2.7 Å and 2.8 Å) and thereby closely positioned at the Schiff base and the transport site (Fig. 4D). Previously, a tight association between HR and palmitate was demonstrated to affect the photocycle and spectral characteristics of HR (*28*); e.g., removal of palmitate causes a slight decrease of the Schiff base pK_a. Why does HR allow the invasion of bulk water into the extracellular half of its interior compartment by adopting a distinct quaternary structure? A possible clue might be the difficulty in generating high-affinity binding sites for chloride rather than for protons, because proton affinities vary by many magnitudes among individual residues (>10^3 to <10^{-24} M). The proximity of the high-dielectricity bulk phase to the halide transport site in HR diminishes the energetic barrier for transferring a halide ion from the bulk phase and, consequently, should increase the affinity of the transport site for anions.

Chloride pumping by HR. The structure of halorhodopsin in its initial state provides several clues common with BR that corroborate a model of mechanistic equivalence for halide and proton transport: First, the ion to be translocated is ion paired with the Schiff base (HR) or makes a covalent link (BR). Second, the cytoplasmic pathway is closed for ion conduction when considering the initial state of archaeal rhodopsins. Third, the charge distribution of the complex counter ion around the PSB is nearly identical as CL501 virtually replaces the OD1 atom of Asp^{85} in BR. Finally, the single site mutants of BR such as $Asp^{85} \rightarrow$ Thr or $Asp^{85} \rightarrow$ Ser are capable of chloride inward transport like HR (*10*).

After photoisomerization (step I* in Fig. 6B), which causes a rearrangement of the PSB in the subangstrom range, all archaeal rhodopsins form redshifted intermediates (λ_{max} for HR and BR ≈ 600 nm). The structure of a cryotrapped K-like intermediate of BR (*29*) showed that the N–H bond of the Schiff base flips after photoisomerization and inverts the alignment of its dipole moment relative to

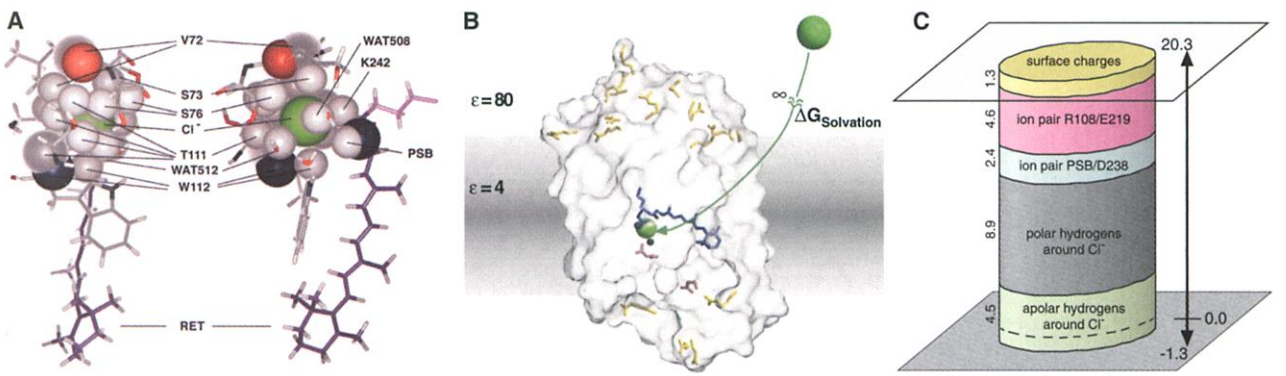

Fig. 5. (**A**) Coordination shell of chloride in the transport site as viewed from two perpendicular directions. CL501 (green) and all residues within 5 Å radius are depicted; contacting atoms (hydrogen, white; carbons, gray; nitrogen, blue; oxygen, red) and CL501 are emphasized as CPK spheres. (**B**) Sketch describing the calculation of free energies for the transfer of chloride from bulk solvent (ε = 80) to the interior of HR. Transfer energies were calculated with MEAD1.1.8 (*39*) with ε = 4 for the protein region and an apolar membrane model that ranged from z = −16 Å to z = +16 Å (PSB nitrogen at z = 0). Partial charges from the protein were subdivided into five sets to separate contributions from different groups on chloride binding: (i) polar and (ii) apolar hydrogen atoms contacting chloride, (iii) the ion pair PSB and Asp^{238}, (iv) the ion pair Arg^{108}-Glu^{219}, and (v) acidic and basic residues on the protein surface. Residues belonging to charge sets iii, iv, and v are highlighted in blue, purple, and yellow, respectively. (**C**) Decomposition of the stabilization energy of chloride in the HR transport site (in kcal/mol). The lower and upper planes correspond to chloride transfer into HR with all partial charges switched on and off, respectively.

Asp[85] without provoking major alterations in the protein environment. Considering HR, this flip should substantially elevate the energy of bound chloride because of an increased electrostatic repulsion with the N → H dipole and the carboxylate of Asp[238]. Only for the next step, the microsecond-range formation of the HR520 intermediate, a first change of chloride interaction with its environment becomes experimentally evident. FTIR spectroscopy showed a concomitant change in the frequencies of the PSB and Arg[108] (*27*) that translates into a loss of the Arg[108]-chloride interaction and strengthening of the PSB-chloride bonding. Likewise, the blueshifted absorption suggests a stabilization of the ground state of HR520 because of a saltlike linkage between the PSB and chloride. According to photovoltaic studies, HR from another Haloarchaeon, *Natronobacterium pharaonis*, transports only 4% of the charge toward the cytosol during the buildup of the HR520 intermediate (*30*). In structural terms, we suggest that this step reflects a passage of the chloride along the N–H dipole of the PSB toward the cytoplasmic side of the retinal chromophore (Fig. 6, A and B). A single serine, Ser[115], which already H bonds to CL501 in the initial state, might be instrumental to keep the chloride solvated; its hydroxyl is suitably positioned above the PSB group to maintain a polar interaction with the chloride during most of its passage. Because of the lack of an HR520 structure, the final position of the chloride after its passage cannot yet be precisely defined, but it probably involves H bonding to the hydroxyl of the conserved residue Thr[203] and water WAT506. WAT506 is the only internal water conserved between HR and BR, and it H bonds to Thr[203], the carbonyl oxygen of Ala[241], and the NE1 atom of Trp[207]. Site-directed mutagenesis of residues on the cytoplasmic side of the chromophore showed only for Thr[203] a role in chloride translocation (*23*), especially for the step of chloride release toward the cytoplasmic surface. The closed cytoplasmic pathway implies not only that chloride stops after its passage but also that HR requires a conformational change to release chloride into the cytosol. In the latter, the changing accessibility toward the cytosol is attributed to a transition between two M states (*2*) before reprotonation of the Schiff base occurs. In HR, experimental data analogously indicated the presence of two HR520 intermediates that differ in the protein and water structure, but not in the location of bound chloride (step S in Fig. 6B) (*31*). As further chloride transport demands proper anion solvation and critical residues other than Thr[203] were found neither by the structure nor by mutagenesis to line such a polar pathway, one has to postulate that a transiently opened cytoplasmic channel allows the entry of water.

Chloride release from the chromophore (step T) leads to the formation of an intermediate, HR640, whose redshifted absorption maximum reflects the lack of interactions between the PSB and an associated counterion (Fig. 6B). Continuing from HR640, the photocycle is finally closed by resealing the cytoplasmic pathway (S), reisomerizing of the chromophore (I), and refilling the transport site with chloride (T).

Symmetry of proton and anion translocation in archaeal rhodopsins. The structures of HR and BR provide an amazing example of the evolutionary economy of nature. Only the replacement of a negatively charged oxygen atom (at Asp[85]) as proton acceptor of BR by chloride in HR changes the kinetic preference and therefore ion specificity completely from cations to anions. It now becomes conceivable how these archaeal rhodopsins alternatively pump protons or chloride ions. After the primary photoisomerization flips the N–H dipole from an extracellular to a cytoplasmic orientation (Fig. 6C), three different scenarios can evolve: In HR, the movable chloride is electrostatically dragged along the PSB by ion-dipole interaction before it is released toward the cytoplasm and a new chloride enters the transport site. In BR, the fixed negative charge of Asp[85] attracts the proton from the PSB for the same energetic reason that chloride moves in HR (Fig. 6C). Then, the

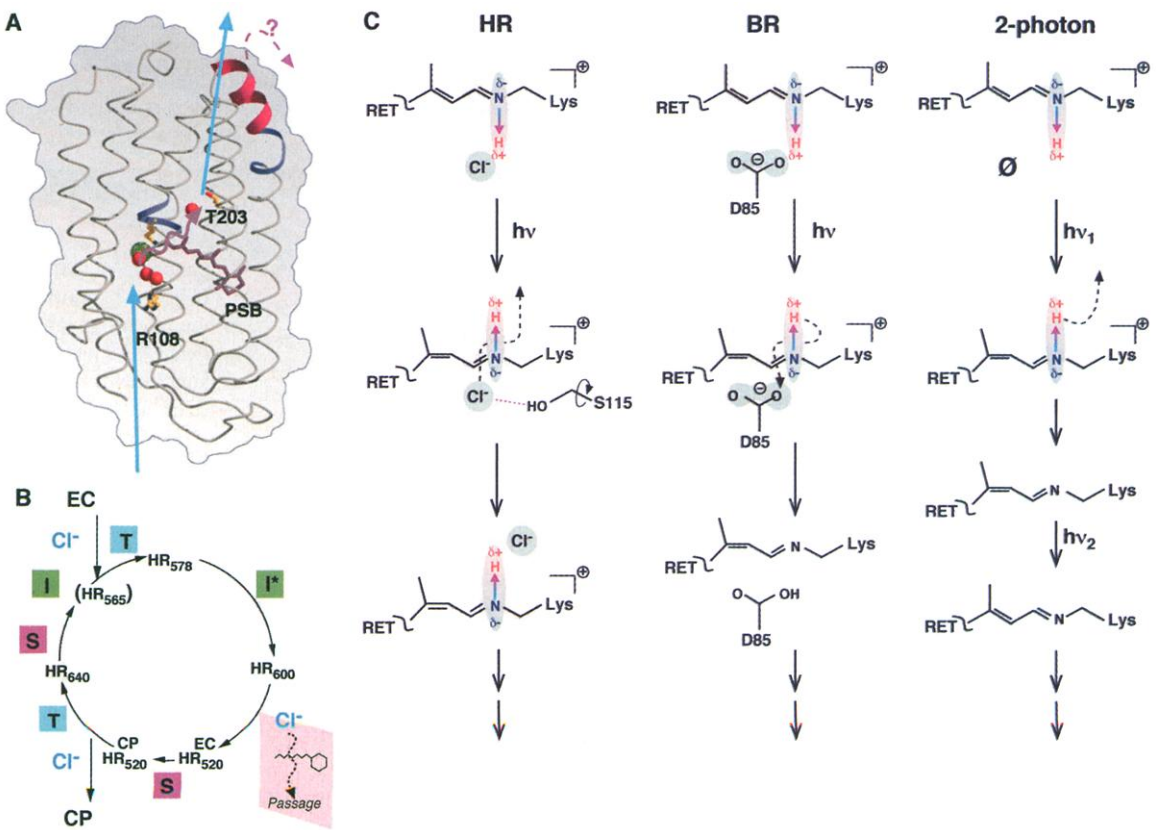

Fig. 6. (**A**) Ion translocation in halorhodopsin. Structural features that probably undergo conformational changes during the photocycle are highlighted (π bulges Ala[178]-Trp[183] and Phe[240]-Phe[245], blue; COOH-terminus of helix E, red; Arg[108], Thr[203], and PSB, sticks). (**B**) Photocycle of halorhodopsin. The six steps necessary for vectorial catalysis are two isomerization reactions of the chromophore (I and I*), two chloride transfer steps (T), and two changes of ion accessibility at the active site (*40*). The additional passage of chloride for formation of HR520 is indicated. (**C**) An ion-dragging mechanism for light-driven ion pumping in archaeal rhodopsins that is controlled by ion-dipole interactions. In the absence of chloride, the two-photon mode for proton transport operates in HR and the nonprotonable Asp[85] mutants of BR (X is Ser or Thr).

Schiff base receives a proton from the cytoplasm, and Asp^{85} finally releases its proton to the extracellular space. If Asp^{85} is missing, the HR mechanism comes into action also for BR when chloride is present. The third mode of action is active in both molecules when both the fixed charge of Asp^{85} and the movable charge of chloride are missing. After dipole flipping, the Schiff base in its high-energy state releases the proton to the cytoplasmic surface as the only choice to relax thermodynamically. As a result, a proton is picked up from the extracellular space after several intermediary steps and proton translocation is observed with inversed vectoriality.

In summary, the high-resolution structure of HR presented here provides a key to understand this case of active transport in both directions by and on the same molecule. Future crystallographic studies on photointermediates of HR should track chloride on its course through this integral membrane protein after photoexcitation.

References and Notes

1. P. D. Boyer, *Annu. Rev. Biochem.* **66**, 717 (1997).
2. D. Oesterhelt, *Curr. Opin. Struct. Biol.* **8**, 489 (1998).
3. B. P. Rosen *et al.*, *Biochim. Biophys. Acta* **1018**, 203 (1990).
4. M. Ikeda and D. Oesterhelt, *Biochemistry* **29**, 2065 (1990).
5. D. Oesterhelt, *Isr. J. Chem.* **35**, 475 (1995).
6. B. Schobert and J. K. Lanyi, *J. Biol. Chem.* **257**, 10306 (1982).
7. W. Havelka *et al.*, *J. Mol. Biol.* **247**, 726 (1995).
8. T. Arlt *et al.*, *Chem. Phys. Lett.* **241**, 559 (1995).
9. E. Bamberg, J. Tittor, D. Oesterhelt, *Proc. Natl. Acad. Sci. U.S.A.* **90**, 639 (1993).
10. J. Sasaki *et al.*, *Science* **269**, 73 (1995).
11. J. Tittor *et al.*, *J. Mol. Biol.* **271**, 405 (1997).
12. HR (mature form: 253 amino acids, molecular mass = 26,962 daltons) was homologously overexpressed in the *H. salinarum* strain D2 as described (*32*). DNA sequencing of the *hop* gene showed a single point mutation, $Val^{229} \rightarrow$ Ala, which is located in a functionally unimportant region of the FG loop. Isolation and purification of the membrane fraction containing HR were performed according to (*33*). HR, solubilized in 5% (w/v) cholate, 4 M KCl, and 50 mM tris-HCl (pH 7.2), was applied to a phenyl-sepharose CL-4B column (Pharmacia), washed with 0.4% (w/v) cholate buffer, and eluted by changing to 1% (w/v) β-octyl-glucoside in the same buffer. HR was concentrated on 50-kD cutoff membrane filters (Amicon) and batchwise incorporated into a cubic lipidic phase as previously described (*14*). Optimal crystallization conditions were found at a final composition of 58 to 62% (w/w) 1-monooleoyl-*rac*-glycerol, 4 M KCl, HR (3.3 to 4.0 mg/ml), and 50 mM tris-HCl (pH 6.5 to 7.4) (22°C, dark). Small crystals of HR formed within 2 weeks and attained final sizes of 0.1 mm by 0.1 mm by 0.02 mm.
13. L.-O. Essen *et al.*, *Proc. Natl. Acad. Sci. U.S.A.* **95**, 11673 (1998).
14. E. Landau and J. P. Rosenbusch, *Proc. Natl. Acad. Sci. U.S.A.* **93**, 14532 (1996).
15. J. Barauskas *et al.*, *Chem. Phys. Lipids* **97**, 167 (1999).
16. H. Luecke *et al.*, *J. Mol. Biol.* **291**, 899 (1999).
17. H. Belrhali *et al.*, *Struct. Folding Des.* **7**, 909 (1999).
18. I. Pascher *et al.*, *Biochem. Biophys. Acta* **1113**, 339 (1992).
19. K. Ihara *et al.*, *J. Mol. Biol.* **285**, 163 (1999).
20. J. Otomo, *Biophys. Chem.* **56**, 137 (1995).
21. D. Okuno *et al.*, *Biochemistry* **38**, 5422 (1999).
22. T. Alshuth *et al.*, *FEBS Lett.* **179**, 55 (1985).
23. M. Rüdiger and D. Oesterhelt, *EMBO J.* **16**, 3813 (1997).
24. T. J. Walter and M. S. Braiman, *Biochemistry* **33**, 1724 (1994).
25. B. Schobert *et al.*, *J. Biol. Chem.* **261**, 2690 (1986).
26. M. Rudiger *et al.*, *EMBO J.* **14**, 1599 (1995).
27. M. S. Braiman, T. J. Walter, D. M. Briercheck, *Biochemistry* **33**, 1629 (1994).
28. A. Corcelli *et al.*, *Biochim. Biophys. Acta* **1281**, 173 (1996).
29. K. Edman *et al.*, *Nature* **401**, 6755 (1999).
30. I. V. Kalaidzidis *et al.*, *FEBS Lett.* **427**, 59 (1998).
31. Y. S. Chon *et al.*, *Biochemistry* **38**, 9449 (1999).
32. J. A. W. Heymann, W. A. Havelka, D. Oesterhelt, *Mol. Microbiol.* **7**, 623 (1993).
33. A. Duschl, M. A. McCloskey, J. K. Lanyi, *J. Biol. Chem.* **263**, 17016 (1988).
34. Single-letter abbreviations for the amino acid residues are as follows: A, Ala; C, Cys; D, Asp; E, Glu; F, Phe; G, Gly; H, His; I, Ile; K, Lys; L, Leu; M, Met; N, Asn; P, Pro; Q, Gln; R, Arg; S, Ser; T, Thr; V, Val; W, Trp; and Y, Tyr.
35. P. J. Kraulis, *J. Appl. Crystallogr.* **24**, 946 (1991).
36. V. Reat *et al.*, *Proc. Natl. Acad. Sci. U.S.A.* **95**, 4970 (1998).
37. M. Colella *et al.*, *Biochim. Biophys. Acta* **1370**, 273 (1998).
38. M. Kolbe, H. Besir, L.-O. Essen, D. Oesterhelt, data not shown.
39. D. Bashford and K. Gerwert, *J. Mol. Biol.* **224**, 473 (1992).
40. U. Haupts *et al.*, *Biochemistry* **36**, 2 (1997).
41. A. G. W. Leslie, in *Joint CCP4 and ESF-EACMB Newsletter on Protein Crystallography No. 26* (Daresbury Laboratory, Warrington, UK, 1992), pp. 44–51.
42. CCP4, *Acta Crystallogr. D* **50**, 760 (1994).
43. A. T. Brünger *et al.*, *Acta Crystallogr. D* **54**, 905 (1998).
44. G. Varo *et al.*, *Biophys. J.* **68**, 2062 (1995).
45. R. A. Laskowski *et al.*, *J. Appl. Crystallogr.* **26**, 283 (1993).
46. A. Nicholls, K. A. Sharp, B. Honig, *Proteins* **11**, 281 (1991).
47. M. R. Gunner, unpublished data.
48. P. Tavan, K. Schulten, D. Oesterhelt, *Biophys. J.* **47**, 415 (1985).
49. P. Beroza and D. A. Case, *J. Phys. Chem.* **100**, 20156 (1996).

50. The authors are very grateful for support by H. Bartunik at synchrotron beamline BW6, Max-Planck groups for structural molecular biology, Hamburg, W. Burmeister at ID14-3, European Synchrotron Radiation Facility Grenoble, and J. Tittor for discussion and DNA sequencing. This work was supported by EU grant BIO4-CT98-0415, Sonderfarschungsbereich 533 (Deutsche Forschungsgemeinschaft), and the Fonds der Chemischen Industrie. Coordinates and structure factors are available from the Protein Data Bank (accession number 1E12).

3 March 2000; accepted 1 May 2000

REPORTS

Anomalous Polarization Profiles in Sunspots: Possible Origin of Umbral Flashes

H. Socas-Navarro,[1] J. Trujillo Bueno,[1,2] B. Ruiz Cobo[1,3]

We present time-series spectropolarimetric observations of sunspots in the Ca II infrared triplet lines, which show a periodic occurrence of anomalous, asymmetric, circular polarization profiles in the umbral chromosphere. The profiles may be caused by the periodic development of an unresolved atmospheric component in a downward flowing magnetized environment. This active component with upward directed velocities as high as 10 kilometers per second is connected to the umbral flash (UF) phenomenon. We can explain the observations with a semiempirical model of the chromospheric oscillation and of the sunspot magnetized atmospheric plasma during a UF event.

Sunspots provide us with a unique example of a magnetically structured plasma through the study of which we may hope to understand a variety of radiation magnetohydrodynamic phenomena. Of particular interest in this respect are the sunspot chromospheric oscillations and the UFs (*1*–*4*). Presently considered as one of the most dramatic dynamic phenomena that take place in sunspots (*5*), UFs have traditionally been associated with the release of large amounts of thermal energy in the chromosphere (*6*). The most relevant known facts about UFs may be summarized as follows (*1*, *2*): UFs consist of the sudden core brightening of the intensity profiles in the chromospheric Ca II lines observed in the umbra of some sunspots. The lines rapidly develop a blueshifted emission core, which reaches a maximum intensity and later disappears, the line profile returning to its quiet preflash shape. The horizontal spatial extent of UFs varies between about 2000 and 3500 km. The rise time of the flash, from the beginning to the phase of maximum intensity, is about 20 to 30 s. The decay back to the quiet state is slower, about 1 min. UFs

[1]Instituto de Astrofísica de Canarias, E-38200 La Laguna, Tenerife, Spain. [2]Consejo Superior de Investigaciones Científicas, Spain. [3]Departamento de Astrofísica, Universidad de La Laguna, Tenerife, Spain.